IEEE Access
Multidisciplinary ⋮ Rapid Review ⋮ Open Access Journal

Received 31 October 2025, accepted 12 November 2025, date of publication 17 November 2025,
date of current version 24 November 2025.

Digital Object Identifier 10.1109/ACCESS.2025.3633806

RESEARCH ARTICLE

A Low-Profile Printed Near-Field Metasurface for Enhanced Far-Field Radiation in Aperture-Type Antennas

MD YEAKUB ALI[1,2], (Student Member, IEEE), KHUSHBOO SINGH[3], (Member, IEEE), SLAWOMIR KOZIEL[4,5], (Fellow, IEEE), ANNA PIETRENKO-DABROWSKA[5], (Senior Member, IEEE), MOHAMMAD NASRAT ZAQUMI[1], AND SUBHAS MUKHOPADHYAY[1], (Fellow, IEEE)

[1]School of Engineering, Macquarie University, Sydney, NSW 2109, Australia
[2]Department of Electronics and Telecommunication Engineering, Rajshahi University of Engineering and Technology, Rajshahi 6204, Bangladesh
[3]School of Electrical and Data Engineering, University of Technology Sydney (UTS), Sydney, NSW 2007, Australia
[4]Department of Engineering, Reykjavik University, 102 Reykjavik, Iceland
[5]Faculty of Electronics, Telecommunications and Informatics, Gdańsk University of Technology, 80-233 Gdańsk, Poland

Corresponding author: Md Yeakub Ali (mdyeakub.ali@students.mq.edu.au)

This work was supported in part by Macquarie University International Research Stipend Program (RTP) Scholarship funded by the Commonwealth Government, Australia; in part by the Icelandic Research Fund under Grant 2410297; and in part by the National Science Centre of Poland under Grant 2022/47/B/ST7/00072.

ABSTRACT A low-profile, single-layer printed metasurface is presented for near-field phase correction in aperture-based antennas to enhance far-field radiation performance. A novel unit cell design is introduced for the phase-correcting metasurface with significantly reduced thickness. Each unit cell consists of a single-layer dielectric substrate with a metallic square loop at the center, surrounded by four L-shaped patches at the corners, printed on both the top and bottom surfaces. The printed metasurface is designed based on the principle of near-field phase transformation. Compared with existing multilayer metallic or printed phase-correcting metasurfaces, the proposed single-layer design significantly reduces the profile, fabrication complexity, weight, and cost while providing improved performance. As a proof of concept, a prototype metasurface was designed, fabricated, and experimentally validated with a resonant cavity antenna of aperture size of $4\lambda_0$ at 12 GHz. The weight of the fabricated metasurface is only 29.2 grams. Measurements demonstrated that after near-field phase correction, the antenna gain improved by 7.35 dB (from 13.75 dBi to 21.1 dBi) with an aperture efficiency of 80.1% at 12 GHz, showing excellent agreement with simulations.

INDEX TERMS Near-field phase transformation (NFPT), non-uniform near-field phase distribution, printed phase-correcting metasurface (PPCM), printed circuit board (PCB), resonant cavity antenna (RCA).

I. INTRODUCTION

Low-profile and lightweight antenna solutions with high performance are crucial for the advancement of modern wireless communication systems, such as satellite reception, point-to-point microwave links, and wireless backhaul networks, where long-distance and uninterrupted service is required [1], [2], [3]. Traditional high-gain solutions include parabolic reflector antennas [4], [5], which are inherently non-planar, bulky and heavy. Another commonly used approach is antenna arrays, which require complex feeding networks. These networks become increasingly lossy at higher frequencies, thereby reducing system efficiency. Transmitarrays (TAs) [6], [7], [8] and reflectarrays (RAs) [9], [10] have also been widely explored to achieve high gain. However, they require a focal distance between the feed and array, increasing the overall height of the antenna system [11], [12], [13].

The associate editor coordinating the review of this manuscript and approving it for publication was Davide Ramaccia.

In recent years, resonant cavity antennas (RCAs) also known as electromagnetic bandgap (EBG) antennas [14] or 2-D leaky-wave antennas have gained significant attention due to their advantages such as planar structure, simplified feeding mechanisms, and ease of fabrication [15]. These antennas achieve enhanced radiation by forming a resonant cavity between a ground plane acting as a perfect reflector and a partially reflective surface (PRS), with their spacing typically close to half a wavelength in free space. However, the transverse propagation of energy from the feed source leads to a non-uniform aperture phase distribution, which degrades the far-field radiation characteristics of conventional RCAs [2]. Although lens-based techniques such as dielectric or printed planar lenses are widely used for phase equalization, they rely on ray-optics principles and assume a point-source feed. This assumption is not applicable for resonant cavity antennas, where the aperture field exhibits a continuous near-field phase distribution governed by cavity resonance. Hence, such lenses are ineffective in this context, motivating the use of a phase-correcting metasurface for direct near-field phase compensation [16].

To address this issue, near-field phase-correcting metasurfaces (PCMs) have recently been introduced as a promising solution [2], [17], [18]. A metasurface is an artificially engineered periodic structure designed to manipulate the properties of electromagnetic waves [13]. PCMs are designed using near-field phase transformation (NFPT) method, which transforms a highly non-uniform aperture phase distribution into a more uniform one, thereby enhancing the far-field performance. A key advantage of this method is that the PCM is placed in the near-field region, at a sub-wavelength distance from the antenna aperture, allowing phase correction without significantly increasing the overall antenna profile [19].

Phase-correcting metasurfaces can generally be classified into dielectric, metallic, or printed types, depending on the materials and fabrication technologies involved. A non-planar dielectric metasurface in [16] improved antenna performance but had a height of 39 mm ($\approx\lambda_0$), making it unsuitable for low-profile applications. A planar dielectric metasurface in [20] offered reduced height, but remained relatively thick and susceptible to damage due to the limitations of conventional manufacturing. Metallic metasurfaces were presented in [2], [17], [21], [22], and [23] for far-field radiation enhancement. Although these designs are more mechanically robust and cost-effective, they consist of multiple layers separated by air gaps, which increases the overall metasurface height and complicate fabrication. 3D-printed all-dielectric metasurfaces were explored in [19], [24], and [25], taking advantage of commercially available low-cost commonly used filaments. While they reduce manufacturing costs, their heights remain relatively large which increases overall antenna profile.

Printed multilayer near-field metasurfaces in [26], [27], and [28] with air gaps between layers improved radiation performance. However, air gaps between layers and the use of spacers or screws not only increase the overall antenna height but also affect the overall performance. Air-gap-free multilayer designs bonded with prepreg have been proposed in [18] and [29], but they require specialized bonding, and their total height is approximately twice that of a single-layer counterparts. In [30] and [31], authors presented compact RCAs with single-layer printed metasurface-based PRS, but they are not high-gain antennas (gain < -15 dBi).

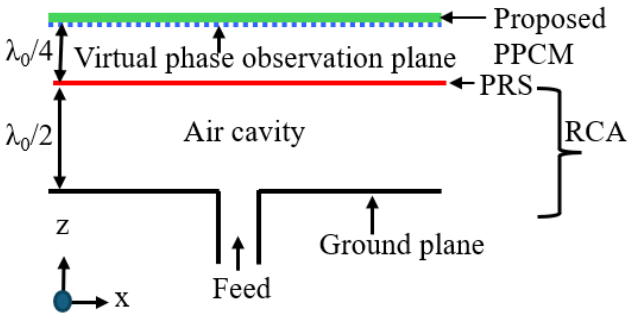

FIGURE 1. Conceptual illustration of a conventional RCA with the proposed PPCM.

In this paper, we present a novel, planar, ultra-thin, single-layer printed phase-correcting metasurface for near-field phase correction in a resonant cavity antenna. To the best of our knowledge, high gain (>20 dBi) RCAs with a single-layer PPCM have not been previously explored and implemented. The proposed PPCM has a thickness of only 1.59 mm ($0.064\lambda_0$), which is significantly thinner than existing counterparts. Compared to multilayer or thicker phase-correcting structures, the proposed design offers a lower profile, reduced weight, and simplified fabrication, while maintaining high performance. Furthermore, the proposed unit cells can compress the profile not only in phase-corrected antenna designs but also in future near-field metasteering systems. This advancement opens new avenues for cost-efficient passive near-field phase transformation and metasteering technologies for high-performance antennas.

The remainder of this paper is organized as follows: Section II outlines the design methodology of the proposed PPCM. Section III details the design of the base antenna, unit cell, and the metasurface. Section IV presents and discuss simulation and measurement results, followed by the conclusion in Section V.

II. METHODOLOGY OF NEAR-FIELD PHASE-CORRECTION

The near-field phase transformation technique [22], [32] is employed to correct the non-uniform phase distribution in the near-field region above the antenna aperture. To briefly explain this technique, a conceptual view of a traditional RCA with the proposed PPCM is shown in Fig. 1. In this method, a near-field phase-correcting metasurface is placed in the near-field region above the antenna aperture. The metasurface locally manipulates the phase of the radiated electric fields from the RCA, such that the resulting near-field distribution at the antenna aperture becomes more uniform.

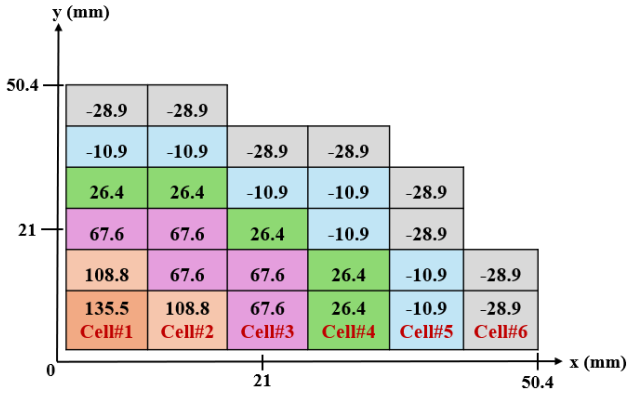

FIGURE 2. Phase distribution in one quadrant of the aperture, cell with the same background color indicate identical phase values, corresponding to identical unit cells.

To design the metasurface, the dominant electric field (E-field) (E_y) phase was extracted from full-wave electromagnetic simulations. To probe the E-field phase, a virtual plane parallel to the aperture was defined at a distance of $\lambda_0/4$, where λ_0 presents the free-space operating wavelength. This distance corresponds to the physical location of the proposed PPCM. This virtual plane was divided into a 2-D square grid with a cell size of $\lambda_0/3$, corresponding to the size of unit cell. The E-field phase was sampled at the center of each grid cell along the x-axis. Further details about metasurface design using NFPT technique are available in [12], [13], and [22]. Due to the circular symmetry of the phase distribution over the aperture [13], the phases were probed only at the center of cells 1 through 6, illustrated in Fig. 2. The extracted near-field phase distribution over one quadrant is also shown in Fig. 2.

A reference phase (θ_0) was selected to achieve more uniformity in phase across the aperture. The required transmission phase delay (θ_r) for each cell was computed as the difference between the reference phase and the probed phase (θ_i), i.e., $\theta_r = \theta_0 - \theta_i$. Unit cell geometries were then selected from the precomputed simulation database to realize the required phase delay. The design steps of near-field phase-correcting metasurface is summarized using a flowchart shown in Fig 3. The required phase delays are summarized in Table 1.

III. RESONANT CAVITY ANTENNA DESIGN WITH PPCM

The design details of the base antenna, unit cell and the proposed PPCM are discussed in the following subsections sequentially.

A. BASE ANTENNA

The proposed single-layer printed phase-correcting metasurface is applicable to any aperture-type antenna that exhibit highly non-uniform electric field phase distributions. As a proof of concept, the PPCM was implemented in this work for a resonant cavity antenna.

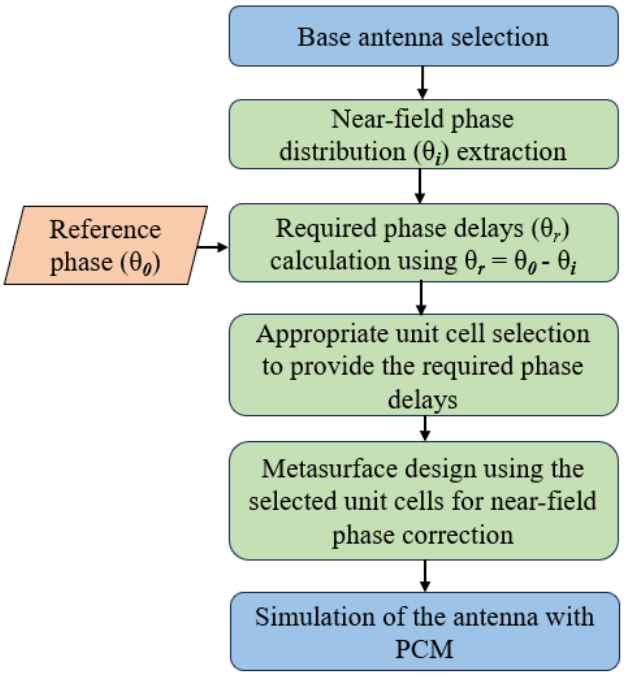

FIGURE 3. Flowchart showing the summary of PCM design steps.

The RCA comprises a metallic, fully reflective circular ground plane and a PRS placed parallel to it. Both the ground plane and the PRS have the same diameter of 100.8 mm ($\approx 4\lambda_0$). A commercial off-the-shelf unprinted dielectric slab made of Rogers TMM4 ($\varepsilon_r = 4.7$, $\tan\delta = 0.002$) with a thickness of 3.175 mm ($\approx \lambda_g/4$) was used as the PRS [2], [33], where λ_0 and λ_g denote the free-space and guided wavelengths at the operating frequency of 12 GHz, respectively. The separation between the ground plane and PRS was set to $\lambda_0/2$ to create resonance within the cavity at the design frequency, thereby enhancing the far-field characteristics [2]. A WR-75 waveguide-to-coaxial adapter was used to excite the cavity through a rectangular slot ($13.05 \times 8.53\ mm$) at the center of the ground plane.

B. UNIT CELL DESIGN AND ANALYSIS

The fundamental element designed to control the electromagnetic wave properties is referred to as a unit cell (UC). A novel approach has been applied to develop the proposed UC, which comprises a single dielectric substrate with metallic patches printed on both sides. The unit cell size is selected as 8.4 mm ($\approx \lambda_0/3$), based on the recommendation in [2]. A commercially available dielectric laminate, Taconic TLY-5 ($\varepsilon_r = 2.2$, $\tan\delta = 0.0009$), with a thickness of 1.52 mm, was used as the substrate. The top and bottom patches of the UC consist of a square metallic loop in the center surrounded by four L-shaped metallic patches at the corners. The perspective, top and bottom views of the unit cells are illustrated in Fig. 4. While the metallic pattern is the same on both sides, the dimensions differ to enable more control of the transmission phase. The length of the L-shaped

TABLE 1. Required phase delays and corresponding unit cell dimension selection.

Cell #	Center distance of the cell (mm)	Probed phase (θ_i) (°)	Reference phase (θ_o) (°)	Required phase delay ($\theta_r = \theta_0 - \theta_i$) (°)	l (mm)	h (mm)	c (mm)
1	4.2	135.47	354	218.53	5.5	5	3
2	12.6	108.78	354	245.22	5	5	3.5
3	21	67.56	354	286.44	4.52	5	1
4	29.4	26.44	354	327.56	4.7	5	4.2
5	37.8	-10.89	354	4.89	1.5	4.5	4.2
6	46.2	-28.93	354	22.93	3.9	1.5	4.2

Note: Center distance of the cell = the distance between the center of the aperture and center of the unit cells along the x-axis, shown in Fig. 2.

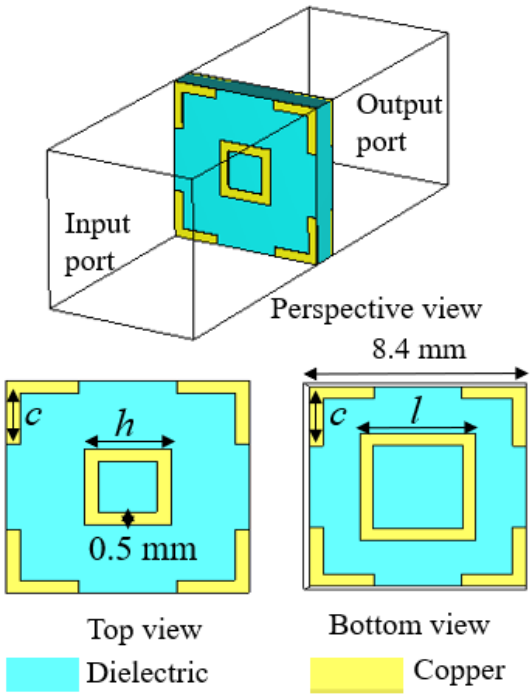

FIGURE 4. Perspective, top, and bottom views of the unit cell in the simulation environment.

corner patches (c) and the central metallic segments (h on the top and l on the bottom) were varied to achieve desired transmission phase delay for near-field phase correction. The UC was simulated using Floquet port excitation under unit cell boundary conditions. A parametric sweep was performed over the geometric parameters l, h, and c to generate a database of transmission magnitude and phase. From this database, the optimal dimensions were selected to provide the desired transmission phase response with high transmission magnitude ($|S_{21}|$).

The geometric dimensions of the unit cells designed to provide the required transmission phase shifts for cells 1 through 6, along with their corresponding transmission magnitudes and phases at 12 GHz, are listed in Table 1. Fig. 5 presents the simulated transmission magnitude ($|S_{21}|$) and phase ($\angle S_{21}$) of the unit cells with the variation of frequency. All the unit cells have higher transmission efficiency, with ($|S_{21}| > -1.95$ dB) at 12 GHz.

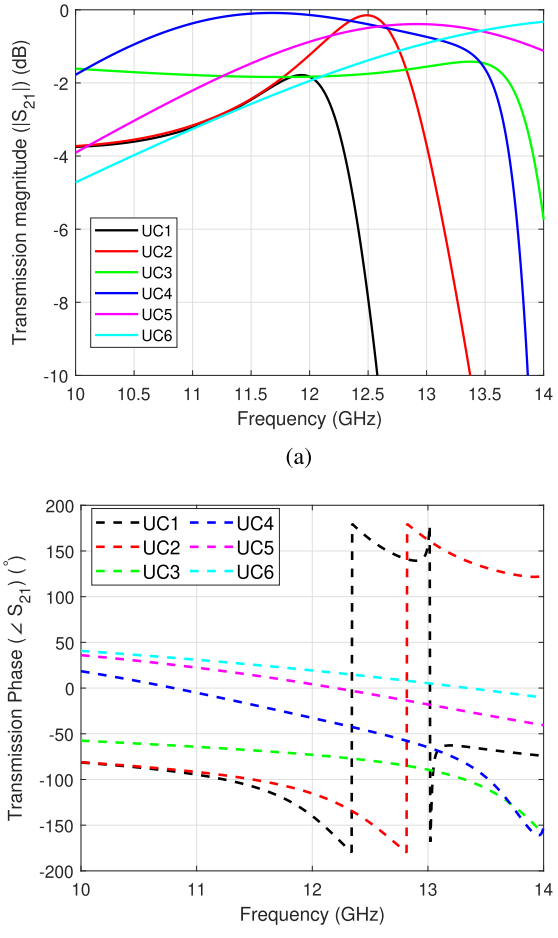

FIGURE 5. Transmission (a) magnitude ($|S_{21}|$) and (b) phase ($\angle S_{21}$) of the unit cells versus frequency.

C. PROPOSED PPCM DESIGN AND FABRICATION

The diameter of the proposed phase-correcting metasurface is equal to that of the RCA ground plane. As discussed in Section II, the six distinct unit cells were selected to provide the required phase delays to the position of the cell 1 to 6 shown in Fig. 2. These unit cells were replicated following a concentric-circular and symmetric pattern to complete the full PPCM design.

Top and bottom views of the fabricated prototype of the proposed metasurface are shown in Fig. 6(a). The proposed

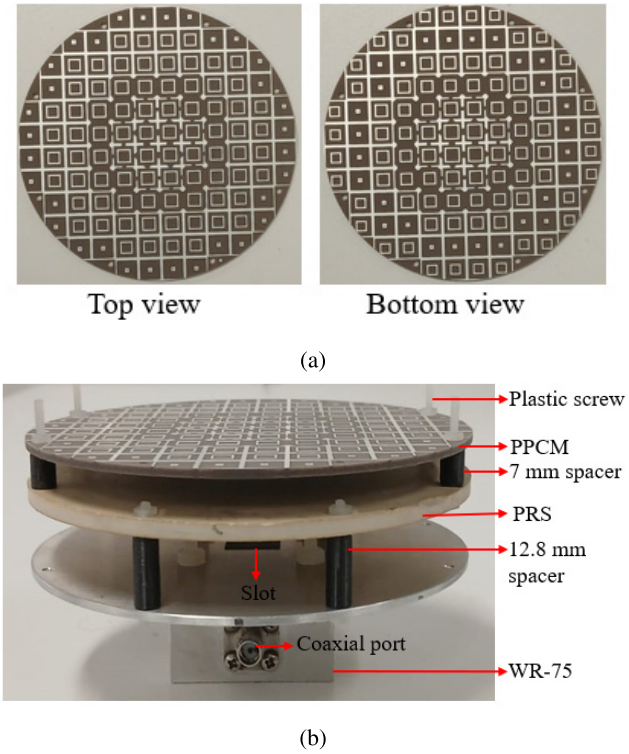

FIGURE 6. (a) Top and bottom views of the fabricated PPCM. (b) Assembled prototype of the RCA loaded with the proposed PPCM.

printed metasurface was fabricated using printed circuit board (PCB) technology. The fully assembled prototype of the RCA incorporating the proposed PPCM is shown in Fig. 6(b). The PPCM and PRS were mechanically supported using 3-D printed spacers made from PLA filament to maintain the optimized interlayer spacing. Specifically, the distance between the ground plane and the PRS and between the PRS and the PPCM were tuned to 12.8 mm and 7 mm, respectively, to achieve optimal performance at the design frequency.

IV. SIMULATED AND MEASURED RESULTS

The proposed PPCM integrated with a resonant cavity antenna was simulated using the time domain solver in CST Microwave Studio (CST-MWS). To validate the simulation results, a prototype was fabricated, as shown in Fig. 6(b), and measured in an NSI anechoic chamber. A photograph of the proposed antenna under test (AUT) setup is shown in Fig. 7. The realized gain of the RCA was calculated using a standard horn antenna as a reference [34].

The dominant E-field component (E_y) of the base antenna was numerically extracted at a distance of $\lambda_0/4$ above the antenna aperture in the xy-plane at 12 GHz using 3D full-wave simulations. The corresponding phase distribution was also extracted after applying the proposed PPCM to evaluate its phase-correcting capability.

Figure 8 shows the one-dimensional (1D) phase distribution along the aperture centerline before and after phase correction. Without the PPCM, the phase distribution

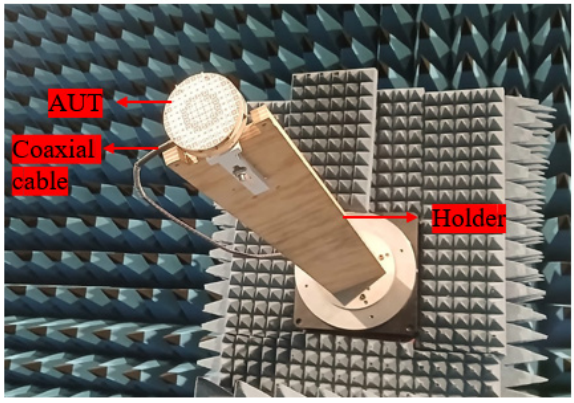

FIGURE 7. Photograph of the proposed antenna under test in an anechoic chamber.

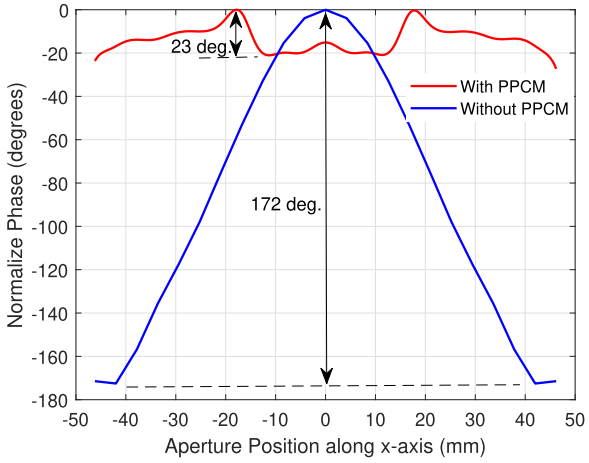

FIGURE 8. 1D phase distribution (along the x-axis) of the RCA, before and after loading the PPCM.

is highly non-uniform, exhibiting a phase variation of approximately 172° across the aperture. This non-uniformity indicates that different parts of the aperture radiate out of phase, causing destructive interference in the far field and consequently degrading the directivity and gain. In contrast, after integrating the PPCM, the phase variation is significantly reduced to about 23°, producing a much flatter phase front. This reduction in phase error demonstrates that the PPCM effectively transforms the highly non-uniform near-field phase into a nearly uniform distribution, thereby improving far-field radiation performance.

The two-dimensional (2D) electric-field phase and magnitude distributions before and after applying the PPCM are presented in Fig. 9. Before correction, strong phase gradients can be observed across both the x- and y-directions. After correction, the phase front becomes considerably smoother and more uniform across the entire aperture, confirming that the PPCM successfully transform the highly non-uniform phase into a more uniform phase. This improved phase uniformity directly leads to enhanced far-field radiation and increased directivity. In addition, the magnitude distribution after phase correction also exhibits a slightly smoother

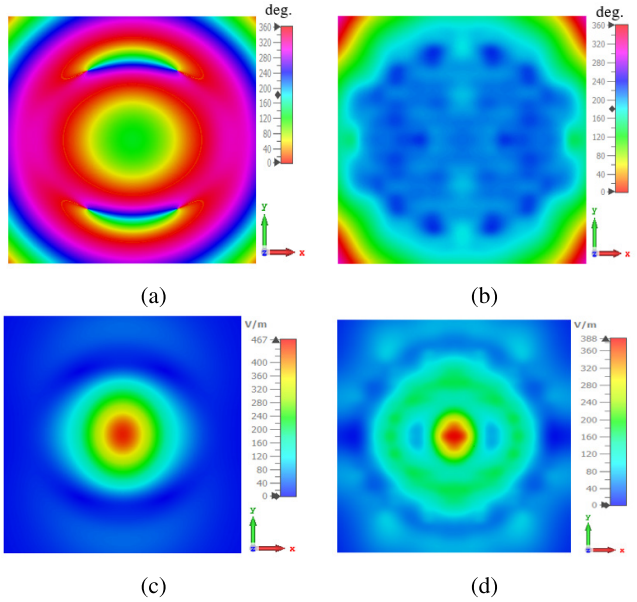

FIGURE 9. 2D electric-field phase and magnitude distributions above the aperture: (a) phase before correction, (b) phase after correction, (c) magnitude before correction, and (d) magnitude after correction with the PPCM.

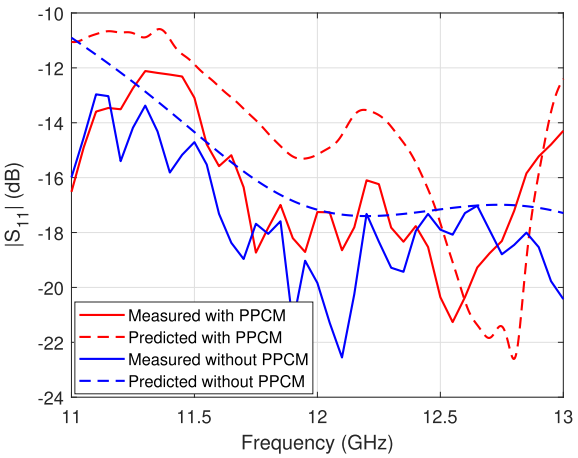

FIGURE 10. Measured and simulated input reflection coefficient ($|S_{11}|$) of the RCA, with and without the PPCM.

profile, indicating a more balanced field distribution across the aperture.

The input reflection coefficient ($|S_{11}|$) of the RCA, both with and without the proposed PPCM, was measured using a vector network analyzer (Keysight PNA N5225B) and compared with the simulation results, as shown in Fig. 10. Both the simulated and measured $|S_{11}|$ values remain below -10 dB throughout the whole operational bandwidth, confirming good impedance matching. Notably, the measured results exhibit better performance than the simulations, indicating excellent impedance matching of the fabricated prototype and validating the accuracy of the design.

Fig. 11 presents the realized gain comparison of the RCA at 12 GHz in both the E- and H-planes before and after near-field phase-correction with the proposed PPCM. Before phase

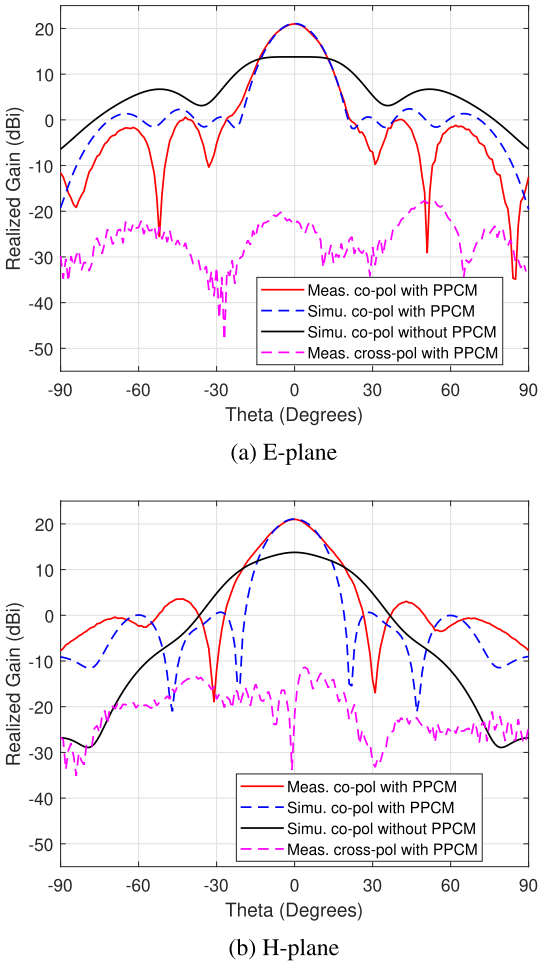

FIGURE 11. Realized gain comparison of the RCA with and without PPCM at 12 GHz.

correction, the gain is 13.75 dBi; this increases significantly to 21.1 dBi when the PPCM is loaded, representing a gain enhancement of 7.35 dB. This improvement is primarily attributed to the more uniformity in phase distribution by the PPCM. The side lobe levels (SLLs) are 21 dB and 18 dB below the main lobe in the E- and H-planes, respectively. The measured results show a good alignment with the simulations. Furthermore, the measured cross-polarization components are 40 dB and 30 dB lower compared to the co-polarization components in E- and H-planes, respectively, indicating effective suppression of undesired radiation components.

The measured gain variation of the RCA with the PPCM is presented in Fig. 12. The RCA with PPCM provides peak performance at 12 GHz. The 3-dB gain bandwidth extends from 11.6 GHz to 12.6 GHz, which is equivalent to 8.26%. For comparison, the realized gain characteristics of the RCA without loading the PPCM is also shown in this figure. A good matching is observed between the measured and simulated results, validating the effectiveness of the proposed design.

To evaluate the stability of the RCA performance across the operational bandwidth, both measured and simulated

TABLE 2. Performance comparison of the proposed PPCM-based RCA with several state-of-the-art published works.

Ref.	Freq. (GHz)	Feed Type	PCM Type No. of layers	Peak Gain (dBi)	Gain Improv. (dB)	Aperture Size (mm)	Aperture Effi. (%)	3-dB Dir. BW (%)	Weight (grams)	PCM Thickness (mm)
[35]	12.5	WR-75	Metallic Four layers	19.6	8.5	144 ($6\lambda_0$)	27	10.4	142.4	19.2 ($0.8\lambda_0$)
[32]	12.4	WR-75	Metal-dielectric Single layer	20.7	8.4	100.8 ($4\lambda_0$)	54.6	22.2	-	6.25 ($0.26\lambda_0$)
[36]	7.88	SMA-fed	Printed Two layers	14.9	7.9	80 ($2.1\lambda_0$)	-	10	-	$0.7\lambda_0$
[37]	13.2	WR-75	Printed Multilayers	20.2	8	$5.28\lambda_0$	23	35	-	$0.13\lambda_0$
[2]	11	WR-75	Metallic Three layers	19.4	8.4	131 ($4.8\lambda_0$)	28	9	87	23 ($0.85\lambda_0$)
[27]	5.8	SMA-fed	Printed Two layers	20.8	-	200 ($3.87\lambda_0$)	95	3.4	-	7 ($0.14\lambda_0$)
[29]	11	WR-75	Printed Two layers	20.8	-	162 ($6\lambda_0$)	34.6	11.8	193	3.24 ($0.12\lambda_0$)
[18]	11	SMA-fed	Printed Two layers	19.3	8	163 ($6\lambda_0$)	26	6	190	3.3 ($0.13\lambda_0$)
This work	12	WR-75	Printed Single layer	21.1	7.35	100.8 ($4\lambda_0$)	80.1	8.3	29.2	1.59 ($0.064\lambda_0$)

Note: - = Data not available, Freq. = operating frequency, improv. = improvement, Dir. = Directivity, BW = Bandwidth, Effi. = Efficiency.

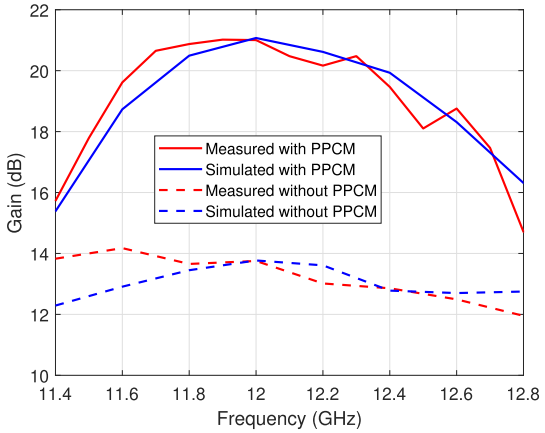

FIGURE 12. Measured and simulated gain variation across the operational bandwidth in the E-plane ($\phi = 90°$).

normalized radiation pattern cuts in the E- and H-planes are presented in Fig. 13 over the frequency range of 11.6 - 12.6 GHz, with a step size 0.2 GHz. The side lobe levels remain at least 10 dB below the main lobe throughout the operating bandwidth in both the E- and H-planes. The measured results are consistent with the simulated results with minor discrepancies.

Table 2 presents a comprehensive comparison between the proposed PPCM-based RCA and several state-of-the-art designs reported in the literature. The comparison includes key parameters such as operating frequency, feed type, metasurface type and number of layers, peak gain, gain improvement, aperture size, aperture efficiency, 3-dB directivity bandwidth, weight, and metasurface thickness. As shown in the table, previous phase-correcting metasurfaces typically consist of either single or multiple PCB or metallic layers, with or without air gaps, which increase fabrication complexity and profile height. In contrast, the

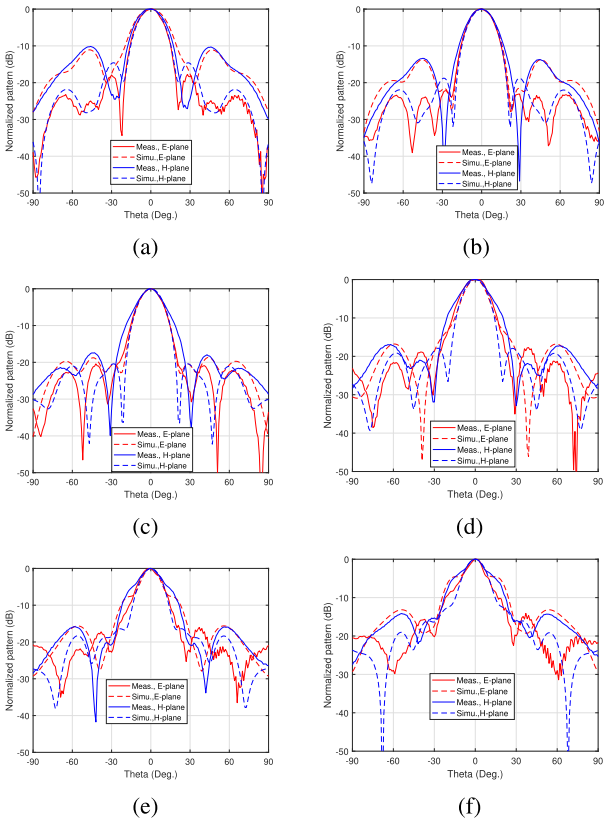

FIGURE 13. Measured and simulated realized gain patterns of the RCA with PPCM in the E- and H-planes at (a) 11.6 GHz (b) 11.8 GHz (c) 12 GHz (d) 12.2 GHz (e) 12.4 GHz (f) 12.6 GHz.

proposed single-layer PPCM achieves higher gain (21.1 dBi) and a gain improvement of 7.35 dB with a significantly reduced thickness of only 1.59 mm ($0.064\lambda_0$). Furthermore, it maintains a competitive aperture efficiency of 80.1%, demonstrating that a low-profile single-layer metasurface can

deliver high-performance near-field phase correction without the complexity of multi-layer implementations.

V. CONCLUSION

Lightweight and low-profile antennas with high gain are important for next-generation wireless communication systems. This paper presented a planar, single-layer, low-profile, and lightweight printed metasurface designed for non-uniform near-field phase correction of aperture-type antennas in order to enhance the far-field directive characteristics. The proposed metasurface effectively reduces antenna profile, fabrication cost, weight, and structural complexity. The fabricated metasurface prototype has a thickness of only 1.59 mm ($0.064\lambda_0$) and a weight of 29.2 grams. Both simulation and experimental results validate the effectiveness of the design. The proposed metasurface enhances the peak gain of a conventional resonant cavity antenna by 7.35 dB and achieves an aperture efficiency of 80.1%, while also reducing sidelobe levels. Furthermore, the proposed metasurface design approach can be extended to realize passive beam-steering systems and multi-beam antenna configurations.

ACKNOWLEDGMENT

The authors would like to thank the UTS Tech Laboratory, Sydney, Australia for giving the opportunity to perform the measurement of the antenna in the anechoic chamber.

REFERENCES

[1] M. I. Nabeel, M. U. Afzal, K. Singh, D. N. Thalakotuna, and K. P. Esselle, "Dual-band printed near-field metasurface with independent phase transformation for enhanced antenna gain," *IEEE Antennas Wireless Propag. Lett.*, vol. 23, pp. 2401–2405, 2024.

[2] A. Lalbakhsh, M. U. Afzal, K. P. Esselle, and S. L. Smith, "Low-cost nonuniform metallic lattice for rectifying aperture near-field of electromagnetic bandgap resonator antennas," *IEEE Trans. Antennas Propag.*, vol. 68, no. 5, pp. 3328–3335, May 2020.

[3] M. Y. Ali, A. Lalbakhsh, K. Singh, S. Koziel, and L. Golunski, "3-D printable metal-dielectric metasurface for Risley prism-based beam-steering antennas," *IEEE Access*, vol. 12, pp. 165143–165154, 2024.

[4] A. Monk, P. Martens, Y. Inasawa, N. Yoneda, I. Naito, M. Miyazaki, Y. Shimawaki, Y. Konishi, A. Iida, and S. Makino, "Ultra-low profile airborne reflector antenna subsystem for broadband satellite communications," in *Proc. 21st Int. Commun. Satell. Syst. Conf. Exhibit*, Apr. 2003, p. 2316.

[5] C. Bruns, P. Leuchtmann, and R. Vahldieck, "Comprehensive analysis and simulation of a 1–18 GHz broadband parabolic reflector horn antenna system," *IEEE Trans. Antennas Propag.*, vol. 51, no. 6, pp. 1418–1422, Jun. 2003.

[6] Y.-M. Cai, K. Li, W. Li, S. Gao, Y. Yin, L. Zhao, and W. Hu, "Dual-band circularly polarized transmitarray with single linearly polarized feed," *IEEE Trans. Antennas Propag.*, vol. 68, no. 6, pp. 5015–5020, Jun. 2020.

[7] A. Aziz, X. Zhang, F. Yang, S. Xu, and M. Li, "A dual-band orthogonally polarized contour beam transmitarray design," *IEEE Trans. Antennas Propag.*, vol. 69, no. 8, pp. 4538–4545, Aug. 2021.

[8] T. K. Pham, L. Guang, D. González-Ovejero, and R. Sauleau, "Dual-band transmitarray with low scan loss for Satcom applications," *IEEE Trans. Antennas Propag.*, vol. 69, no. 3, pp. 1775–1780, Mar. 2021.

[9] Z. Zhang, H. Luyen, J. H. Booske, and N. Behdad, "A dual-band, polarization-rotating reflectarray with independent phase control at each band," *IEEE Trans. Antennas Propag.*, vol. 69, no. 9, pp. 5546–5558, Sep. 2021.

[10] R. L. Farias, C. Peixeiro, and M. V. T. Heckler, "Single-layer dual-band dual-circularly polarized reflectarray for space communication," *IEEE Trans. Antennas Propag.*, vol. 70, no. 7, pp. 5989–5994, Jul. 2022.

[11] X. Zhao, C. Yuan, L. Liu, S. Peng, Q. Zhang, and H. Zhou, "All-metal transmit-array for circular polarization design using rotated cross-slot elements for high-power microwave applications," *IEEE Trans. Antennas Propag.*, vol. 65, no. 6, pp. 3253–3256, Jun. 2017.

[12] F. Ahmed, M. U. Afzal, D. N. Thalakotuna, and K. P. Esselle, "Novel dual-band metascreen for dual-band near-field phase correction," *IEEE Trans. Antennas Propag.*, vol. 71, no. 7, pp. 5591–5604, Jul. 2023.

[13] M. Y. Ali, A. Lalbakhsh, S. Koziel, L. Golunski, F. Ahmed, and M. Asadnia, "A low-profile 3-D printable metastructure for performance improvement of aperture antennas," *Sci. Rep.*, vol. 14, no. 1, p. 17930, Aug. 2024.

[14] Z.-G. Liu, R.-J. Yin, and W.-B. Lu, "A novel dual-band shared-aperture antenna based on folded reflectarray and Fabry–Perot cavity," *IEEE Trans. Antennas Propag.*, vol. 70, no. 11, pp. 11177–11182, Nov. 2022.

[15] M. Akbari, S. Gupta, M. Farahani, A. R. Sebak, and T. A. Denidni, "Gain enhancement of circularly polarized dielectric resonator antenna based on FSS superstrate for MMW applications," *IEEE Trans. Antennas Propag.*, vol. 64, no. 12, pp. 5542–5546, Dec. 2016.

[16] M. U. Afzal, K. P. Esselle, and B. A. Zeb, "Dielectric phase-correcting structures for electromagnetic band gap resonator antennas," *IEEE Trans. Antennas Propag.*, vol. 63, no. 8, pp. 3390–3399, Aug. 2015.

[17] F. Ahmed, M. U. Afzal, T. Hayat, K. P. Esselle, and D. N. Thalakotuna, "A dielectric free near field phase transforming structure for wideband gain enhancement of antennas," *Sci. Rep.*, vol. 11, no. 1, p. 14613, Jul. 2021.

[18] M. U. Afzal and K. P. Esselle, "A low-profile printed planar phase correcting surface to improve directive radiation characteristics of electromagnetic band gap resonator antennas," *IEEE Trans. Antennas Propag.*, vol. 64, no. 1, pp. 276–280, Jan. 2016.

[19] T. Hayat, M. U. Afzal, A. Lalbakhsh, and K. P. Esselle, "Additively manufactured perforated superstrate to improve directive radiation characteristics of electromagnetic source," *IEEE Access*, vol. 7, pp. 153445–153452, 2019.

[20] A. Lalbakhsh, M. U. Afzal, K. P. Esselle, and S. L. Smith, "Wideband near-field correction of a Fabry–Perot resonator antenna," *IEEE Trans. Antennas Propag.*, vol. 67, no. 3, pp. 1975–1980, Mar. 2019.

[21] F. Ahmed, M. U. Afzal, T. Hayat, K. P. Esselle, and D. N. Thalakotuna, "Self-sustained rigid fully metallic metasurfaces to enhance gain of shortened horn antennas," *IEEE Access*, vol. 10, pp. 79644–79654, 2022.

[22] A. Lalbakhsh, M. U. Afzal, T. Hayat, K. P. Esselle, and K. Mandal, "All-metal wideband metasurface for near-field transformation of medium-to-high gain electromagnetic sources," *Sci. Rep.*, vol. 11, no. 1, p. 9421, May 2021.

[23] M. I. Nabeel, M. U. Afzal, K. Singh, D. N. Thalakotuna, and K. P. Esselle, "Waveguide-based all-metal near-field metasurfaces for linearly and circularly polarized beam steering antennas," *IEEE Access*, vol. 13, pp. 10857–10869, 2025.

[24] V. M. Pepino, A. F. da Mota, A. Martins, and B.-H.-V. Borges, "3-D-printed dielectric metasurfaces for antenna gain improvement in the Ka-band," *IEEE Antennas Wireless Propag. Lett.*, vol. 17, pp. 2133–2136, 2018.

[25] T. Hayat, M. U. Afzal, A. Lalbakhsh, and K. P. Esselle, "3-D-printed phase-rectifying transparent superstrate for resonant-cavity antenna," *IEEE Antennas Wireless Propag. Lett.*, vol. 18, pp. 1400–1404, 2019.

[26] M. I. Nabeel, K. Singh, M. U. Afzal, D. N. Thalakotuna, and K. P. Esselle, "A thin transparent phase correction surface for patch antenna gain enhancement," in *Proc. IEEE Int. Symp. Antennas Propag. USNC-URSI Radio Sci. Meeting (USNC-URSI)*, Jul. 2023, pp. 1779–1780.

[27] L. Zhou, X. Duan, Z. Luo, Y. Zhou, and X. Chen, "High directivity Fabry–Perot antenna with a nonuniform partially reflective surface and a phase correcting structure," *IEEE Trans. Antennas Propag.*, vol. 68, no. 11, pp. 7601–7606, Nov. 2020.

[28] L. Zhou, X. Chen, X. Duan, and J. Li, "FPA using a three-layer PSS for gain enhancement," *IET Microw., Antennas Propag.*, vol. 12, no. 3, pp. 400–405, Feb. 2018.

[29] A. Lalbakhsh, M. U. Afzal, and K. P. Esselle, "Multiobjective particle swarm optimization to design a time-delay equalizer metasurface for an electromagnetic band-gap resonator antenna," *IEEE Antennas Wireless Propag. Lett.*, vol. 16, pp. 912–915, 2017.

[30] K. Chen, Z. Yang, Y. Feng, B. Zhu, J. Zhao, and T. Jiang, "Improving microwave antenna gain and bandwidth with phase compensation metasurface," *AIP Adv.*, vol. 5, no. 6, Jun. 2015.

[31] Y. I. Abdulkarim, H. N. Awl, F. F. Muhammadsharif, M. Karaaslan, R. H. Mahmud, S. O. Hasan, Ö. Işık, H. Luo, and S. Huang, "A low-profile antenna based on single-layer metasurface for Ku-band applications," *Int. J. Antennas Propag.*, vol. 2020, pp. 1–8, Dec. 2020.
[32] M. Y. Ali, A. Lalbakhsh, K. Singh, S. H. Taheri, and S. Mukhopadhyay, "A metal-dielectric 3D-printable metastructure for the radiation enhancement of electromagnetic band-gap resonator antennas," *Frontiers Antennas Propag.*, vol. 3, May 2025, Art. no. 1585028.
[33] C. Cheype, C. Serier, M. Thevenot, T. Monediere, A. Reineix, and B. Jecko, "An electromagnetic bandgap resonator antenna," *IEEE Trans. Antennas Propag.*, vol. 50, no. 9, pp. 1285–1290, Sep. 2002.
[34] C. A. Balanis, *Antenna Theory: Analysis and Design*. Hoboken, NJ, USA: Wiley, 2016.
[35] F. Ahmed, K. Singh, K. P. Esselle, and D. Thalakotuna, "Near-field metallic metasurfaces for enhancing antenna capabilities," in *Proc. 5th Austral. Microw. Symp. (AMS)*, Feb. 2023, pp. 53–54.
[36] Z. Ding, J. Cao, D. Zhang, N. Nasimuddin, M. Y. W. Chia, and H. Wang, "A wideband high-gain Fabry–Perot resonator cavity antenna with low-RCS property using metasurface structures," *Results Eng.*, vol. 27, 2025, Art. no. 106647.
[37] T. A. Khan and A. M. H. Wong, "A wideband low-profile phase correcting metasurface to improve directive radiation characteristics of resonant cavity antennas," in *Proc. IEEE Int. Symp. Antennas Propag. INC/USNC-URSI Radio Sci. Meeting (AP-S/INC-USNC-URSI)*, Jul. 2024, pp. 1799–1800.

MD YEAKUB ALI (Student Member, IEEE) received the B.Sc. Engineering degree from the Department of Electronics and Telecommunication Engineering (ETE) and M.Sc. Engineering degree from the Department of Electrical and Electronic Engineering (EEE) from Rajshahi University of Engineering and Technology (RUET), in 2014 and 2020, respectively. He is currently pursuing the Ph.D. degree with the School of Engineering, Macquarie University, Sydney, NSW, Australia.

He was an Engineer with Bangla Trac Communication and Robi Axiata Ltd. from 2014 to 2017. He was a Lecturer with the Department of ETE with Rajshahi University of Engineering and Technology, Rajshahi, Bangladesh, from 2017 to 2021, and he was promoted to an Assistant Professor with the same department from 2021. His research interests include antennas for mobile and satellite communication and metasurfaces for antenna applications.

KHUSHBOO SINGH (Member, IEEE) received the Bachelor of Technology degree (Hons.) in electronics and communication engineering from SHIATS, India, the Master of Science by Research degree in electronics and communication engineering from LNMIIT, in India, and the Ph.D. degree in electrical engineering from Macquarie University, in Australia, focusing on antenna and propagation research. She is a Research Fellow with the University of Technology Sydney. Two main themes that best summarise her recent postdoctoral research endeavors are high-gain, beam-steering antennas and mm-wave high-power planar array antennas. In addition, she is developing reconfigurable intelligent surfaces (RIS) and metasurfaces. She is actively involved in cutting-edge research and collaborates on critical projects with the Defence Science and Technology Group and the NSW government. The Australian government supported her Ph.D. studies via the acclaimed iRTP scholarship initiative, with a near-perfect grade point average (GPA). Her significant contributions to the DSTG Project earned her team "MetaSteerers," the 2023 Eureka Prize for Outstanding Science for Safeguarding Australia. Her master's degree research emphasis on radio-frequency (RF) front-end components that was completely financed by a merit-based LNMIIT Scholarship. She received the Silver Medal during the bachelor's degree.

SLAWOMIR KOZIEL (Fellow, IEEE) received the M.Sc. and Ph.D. degrees in electronic engineering from Gdańsk University of Technology, Poland, in 1995 and 2000, respectively, the M.Sc. degree in theoretical physics and the M.Sc. and Ph.D. degrees in mathematics from the University of Gdańsk, Poland, in 2000, 2002, and 2003, respectively.

He is currently a Professor with the Department of Engineering, Reykjavik University, Iceland. His current research interests include the CAD and modeling of microwave and antenna structures, simulation-driven design, surrogate-based optimization, space mapping, circuit theory, analog signal processing, evolutionary computation, and numerical analysis.

ANNA PIETRENKO-DABROWSKA (Senior Member, IEEE) received the M.Sc. and Ph.D. degrees in electronic engineering from Gdańsk University of Technology, Poland, in 1998 and 2007, respectively. She is currently an Associate Professor with Gdańsk University of Technology. Her research interests include simulation-driven design, design optimization, control theory, modeling of microwave and antenna structures, and numerical analysis.

MOHAMMAD NASRAT ZAQUMI received the master's degree from the King Abdulaziz University, Saudi Arabia, in 2022. He is currently a Ph.D. degree with the School of Engineering, Macquarie University, Sydney, NSW, Australia. His research interests include antenna, metasurface, and metamaterial absorber design.

SUBHAS MUKHOPADHYAY (Fellow, IEEE) received the B.E.E. degree from Jadavpur University, Kolkata, India, the M.E.E. degree from Indian Institute of Science, Bengaluru, India, the Ph.D. degree in engineering from Jadavpur University, Kolkata, and the D.Eng. degree in engineering from Kanazawa University, Japan.

He is currently a Professor of mechanical/electronics engineering with Macquarie University, Australia and the Discipline Leader of the Mechatronics Engineering Degree Program. His fields of interest include Smart Sensors and sensing technology, wireless sensors and network (WSN), the Internet of Things (IoT), wearable sensors, medical devices, mechatronics and robotics. He has supervised 60 postgraduate students and over 200 Honors students. He has examined 90 postgraduate theses.

Dr. Mukhopadhyay is a Fellow of IET (UK), a Fellow of IETE (India), a Topical Editor of IEEE Sensors Journal, an Associate Editor of IEEE Transactions on Instrumentation and Measurements, and IEEE Review of Biomedical Engineering. He is the Editor-in-Chief of the International Journal on Smart Sensing and Intelligent Systems. He was the Founding Chair of the IEEE Sensors Council New South Wales Chapter and IEEE IMS NSW Chapter. He chairs the IEEE IMS NSW chapter.